Atmospheric Environment 146 (2016) 141–152

Contents lists available at ScienceDirect

Atmospheric Environment

journal homepage: www.elsevier.com/locate/atmosenv

Atmospheric mercury measurements at a suburban site in the Mid-Atlantic United States: Inter-annual, seasonal and diurnal variations and source-receptor relationships

Xinrong Ren [a, b, c, *], Winston T. Luke [a], Paul Kelley [a, b], Mark D. Cohen [a], Richard Artz [a], Mark L. Olson [d], David Schmeltz [e], Melissa Puchalski [e], Daniel L. Goldberg [c, 1], Allison Ring [c], Gina M. Mazzuca [c], Kristin A. Cummings [c], Lisa Wojdan [c, 2], Sandra Preaux [c, 3], Jeff W. Stehr [c, 4]

[a] Air Resources Laboratory, National Oceanic and Atmospheric Administration, College Park, MD, USA
[b] Cooperative Institute for Climate and Satellites, University of Maryland, College Park, MD, USA
[c] Department of Atmospheric and Oceanic Science, University of Maryland, College Park, MD, USA
[d] Illinois State Water Survey, University of Illinois at Urbana-Champaign, Champaign, IL, USA
[e] Clean Air Markets Division, Environmental Protection Agency, Washington, DC, USA

HIGHLIGHTS

- Decreases in [GEM], [GOM], [PBM], and Hg wet deposition over 2007–2015 were observed.
- Trajectory analysis shows correlation between Hg emissions and observed mercury.
- Two possible sources of GOM include direct emissions and photochemical oxidation.

ARTICLE INFO

Article history:
Received 14 February 2016
Received in revised form
1 July 2016
Accepted 8 August 2016
Available online 10 August 2016

Keywords:
Atmospheric mercury
Gaseous elemental mercury
Gaseous oxidized mercury
Particulate-bound mercury
Trend
HYSPLIT

ABSTRACT

Different atmospheric mercury forms have been measured at a suburban site in Beltsville, Maryland in the Mid-Atlantic United States since 2007 to investigate their inter-annual, seasonal and diurnal variabilities. Average concentrations and standard deviations of hourly measurements from 2007 to 2015 were 1.41 ± 0.23 ng m^{-3} for gaseous elemental mercury (GEM), 4.6 ± 33.7 pg m^{-3} for gaseous oxidized mercury (GOM), and 8.6 ± 56.8 pg m^{-3} for particulate-bound mercury (PBM). Observations show that on average, the rates of decrease were 0.020 ± 0.007 ng m^{-3} yr^{-1} (or 1.3 ± 0.5% yr^{-1}, statistically significant, p-value < 0.01) for GEM, 0.54 ± 0.19 pg m^{-3} yr^{-1} (or 7.3 ± 2.6% yr^{-1}, statistically significant, p-value < 0.01) for GOM, and 0.15 ± 0.35 pg m^{-3} yr^{-1} (or 1.6 ± 3.8% yr^{-1}, statistically insignificant, p-value > 0.01) for PBM over this nine-year period. In addition, the collocated annual mercury wet deposition decreased at a rate of 0.51 ± 0.24 μg m^{-2} yr^{-2} (or 4.2 ± 1.9% yr^{-1}, statistically insignificant, p-value > 0.01). Diurnal variation of GEM shows a slight peak in the morning, likely due to the shallow boundary layer. Seasonal variation of GEM shows lower levels in fall. Both diurnal variations of GOM and PBM show peaks in the afternoon likely due to the photochemical production of reactive mercury from the oxidation of GEM and the influence of boundary layer processes. Seasonally, GOM measurements show high levels in spring and constant low levels in the other three seasons, while PBM measurements exhibit higher levels from late fall to early spring and lower levels from late spring to fall. These measurement data were analyzed using the HYSPLIT back trajectory model in order to examine possible source-receptor relationships at this suburban site. Trajectory frequency analysis shows that high GEM/

* Corresponding author. NOAA Air Resources Laboratory, 5830 University Research Court, College Park, MD 20740, USA.
E-mail address: xinrong.ren@noaa.gov (X. Ren).
[1] Now at Energy Systems Division, Argonne National Laboratory, Argonne, IL, USA.
[2] Now at Iroquois High School, Elma, New York, USA.
[3] Now at Stinger Ghaffarian Technologies, Greenbelt, Maryland, USA.
[4] Now at Booz Allen Hamilton, Washington, District of Columbia, USA.

http://dx.doi.org/10.1016/j.atmosenv.2016.08.028

GOM/PBM events were generally associated with high frequencies of the trajectories passing through areas with high mercury emissions, while low GEM/GOM/PBM levels were largely associated the trajectories passing through relatively clean areas. This study indicates that local and regional sources appear to have a significant impact on the site and these impacts appear to have changed over time, as the local/regional emissions have been reduced.

1. Introduction

Mercury (Hg) is a ubiquitous and neurotoxic pollutant and exists in the environment for long periods by cycling between the air, water, and soil in different chemical forms. Atmospheric emissions of mercury are important, as atmospheric deposition is the most significant loading pathway for many ecosystems (UNEP, 2013). After deposition to watersheds and receiving waters, mercury can be converted to methylmercury, a highly toxic form. Methylmercury is incorporated into the food chain and increases with trophic levels through bioaccumulation (Morel et al., 1998; Fitzgerald et al., 1998). Humans are exposed to methylmercury primarily through consuming contaminated fish and other aquatic organisms (Sunderland, 2007; Choi and Grandjean, 2008; Selin, 2009). Methylmercury can adversely affect the nervous system, particularly those of fetuses and young children (Choi and Grandjean, 2008).

The chemical composition of atmospheric mercury is not completely known and consists of three operationally defined forms: gaseous elemental mercury (GEM), gaseous oxidized mercury (GOM), and particulate-bound mercury (PBM). The absolute levels and relative proportions of GEM, GOM, and PBM in the atmosphere vary geographically due to different land use patterns, human activities, and numerous physical and chemical processes. GEM is the predominant mercury forms in the atmosphere and typically accounts for >90% of total mercury (Schroeder and Munthe, 1998). Measurements of atmospheric mercury composition and other chemical and meteorological parameters can help us to assess both regional and global atmospheric budgets and cycling of mercury. A declining GEM concentration trend has been observed at many surface sites (Sprovieri et al., 2010; Zhang et al., 2016). In North America, studies have shown the correlation of power-plant emission controls and reducing atmospheric mercury concentrations (Castro and Sherwell, 2015; Zhang et al., 2016), while mercury data observed in China suggest an increasing trend over the last decade (Fu et al., 2015). Long-term monitoring of atmospheric mercury is thus critical to assemble a publicly available data record for model evaluation and to discern trends in atmospheric mercury concentrations. It is also important to establish correlation with meteorology and ancillary trace gases to better understand the emissions, transport, transformation, and fate of mercury in the atmosphere. Ultimately, these investigations can help to elucidate mercury source-receptor relationships so that policy-makers and regulators can assess the impacts of potential changes in mercury emissions with more certainty.

Atmospheric mercury forms have been measured at a suburban site near the Washington Metropolitan area in the Mid-Atlantic United States since 2007. In this work, an analysis of multi-year continuous measurements of atmospheric mercury was performed. Back trajectory simulations were conducted to examine the mercury source-receptor relationships in this suburban environment. The main purpose of this study is to increase understanding of how different processes influence atmospheric mercury concentrations.

2. Measurement and model description

2.1. Site

The monitoring station is located at the National Oceanic and Atmospheric Administration (NOAA)'s Beltsville site near Beltsville, Maryland (39.0284°N, 76.8172°W) on the campus of the United States Department of Agriculture's Beltsville Agricultural Research Center, and bordering the U.S. Fish and Wildlife Service's Patuxent National Wildlife Refuge (NWR). It is one of the National Atmospheric Deposition Program (NADP)'s Atmospheric Mercury Network (AMNet) sites (site ID: MD99). The site is located on an agricultural area embedded within a suburban portion of the Washington, DC metropolitan area and is representative of much of the semi-urban nature of the Chesapeake Bay watershed. The area near the site contains a few small experimental agricultural plots and some small forests. The location of the monitoring site and major regional point sources of mercury are shown in Fig. 1.

A 10-m walk-up tower was established in a clearing surrounded by grassland. All chemical analyzers were housed in a climate-controlled shelter adjacent to the tower. Measurements of atmospheric mercury forms (GEM, GOM, and PBM) were made from the top of the tower with an inlet height of 10.6 m above ground to minimize local surface effects. The site also hosts measurements under the United States Environmental Protection Agency (EPA)'s Clean Air Status and Trends Network (CASTNet) (including meteorological parameters and trace gases that consist of sulfur dioxide (SO_2), ozone (O_3), carbon monoxide (CO, whose measurements were terminated in September 2012), and total reactive nitrogen (NO and NO_y) (US EPA, 2016); NADP's Mercury Deposition Network (MDN) for mercury wet deposition (NADP, 2015); and NADP's National Trends Network (NTN) for major ions in precipitation.

2.2. Measurements

2.2.1. Measurements of mercury forms

At the Beltsville site two Tekran speciation systems (Tekran Instrument Corporation, Ontario, Canada) were used to measure GEM, GOM and PBM over 2007–2015. Each system uses a Tekran 1130/1135 speciation unit coupled with a Tekran 2537 Cold Vapor Atomic Fluorescence Spectrometer (CVAFS). Details of the system have been described by Landis et al. (2002) and Lindberg et al. (2002). Briefly, as ambient air flows through the system, GOM is collected on a KCl-coated annular denuder followed by the collection of PBM (with particle diameter < 2.5 μm) on a quartz regenerable particle filter (RPF) and GEM on gold traps. The collected GOM on the denuder and PBM on the quartz filter are then thermally desorbed and quantitatively converted to GEM, which is then analyzed by the Tekran 2537. Every 2 h each mercury speciation system provides twelve 5-min consecutive GEM measurements

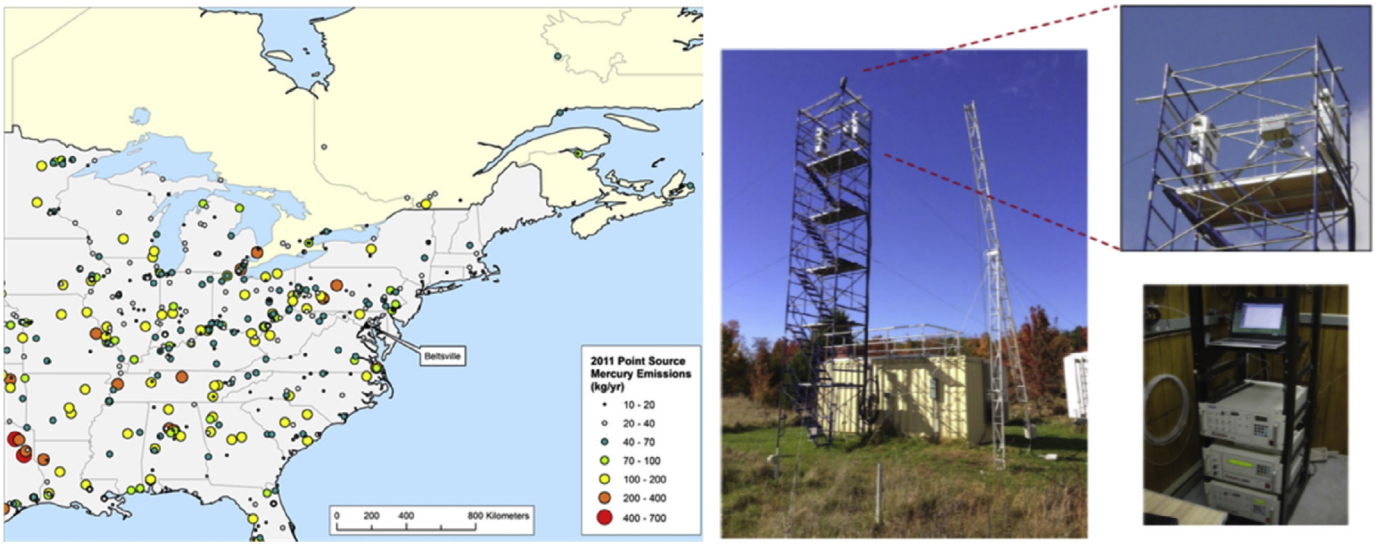

Fig. 1. *Left*: the location of the Beltsville site and major regional mercury point sources with emission rates greater than 10 kg yr^{-1} based on the US EPA's 2011 National Emission Inventory (NEI) and Environment Canada's National Pollutant Release Inventory (NPRI, data downloaded from http://ec.gc.ca/inrp-npri/). *Right*: pictures showing the instrumentation at the Beltsville site.

during the first hour. GOM and PBM are sampled during the first hour and analyzed during the second hour. Because air is only sampled during the first hour of the 2-h period, the two speciation systems, operating asynchronously by 1 h, provided truly continuous measurements of atmospheric mercury speciation. The two collocated mercury speciation systems at the site also provided opportunities to evaluate methodological precision (through synchronous operation) and to test methodological refinements.

It is essential to maintain the Tekran systems properly in order to optimize their performance. The standard protocols for AMNet (Gay et al., 2013) were consistently followed for the operation of the Tekran speciation systems at the Beltsville site over 2007–2015. For example, the soda lime traps that dry air sample for the Tekran 2537 analyzers were changed weekly, the frits at the sample entrance and denuders were changed every 2 weeks, and the RPFs were changed every 4 weeks. All changed glassware was cleaned with diluted nitric acid, rinsed with purified water and then dried with methanol. An air dehumidifier (Tekran Model 1102 Air Dryer) was used to generate zero air. The Tekran 2537 analyzers were calibrated with an internal permeation source to ensure acceptable response factors (>6,000,000 counts per ng of GEM). Quarterly manual-spike Hg tests were conducted by injecting known amounts of GEM into the injection ports on the front panels using a calibrated Hamilton Digital Syringe (Hamilton Company, Reno, NV) and a Tekran Model 2505 Hg vapor calibration unit (Tekran Corporation, Inc., Toronto, Ontario, Canada). The mean recovery of the injected Hg was 100.6 ± 1.8% and 100.5 ± 2.6% for the two Tekran systems, respectively. The detection limit for GEM was about 0.1 ng m^{-3} as determined by the manufacturer. The detection limit for GOM and PBM was about 1.2 pg m^{-3}, determined as the minimum detectable signal (about 1000 counts) plus 3 times the standard deviation of zero flush values that were subtracted from the GOM and PBM. Based on the error propagation method specified by Temme et al. (2007), we estimate the uncertainty of our Hg measurements to be ~8% (2σ). This is similar to the 10% uncertainties obtained from a field intercomparison study (Aspmo et al., 2005).

The use of KCl-coated denuders, either as part of the automated Tekran speciation system or using manual analysis, is the approach that is currently considered to be the standard method for the measurement of GOM. We note, however, that in recent laboratory (Lyman et al., 2010; McClure et al., 2014) and field (Ambrose et al., 2013; Gustin et al., 2013) studies it has been reported that the Tekran 1130 speciation unit may underestimate the atmospheric concentrations of GOM. McClure et al. (2014) found that ozone and humidity cause a low collection efficiency of GOM on KCl-coated denuders due to the release of gaseous elemental Hg from the denuder. It is not clear if the results from this field instrument intercomparison study can be generalized to all field measurements (Castro and Sherwell, 2015) and there were other problems (e.g., production of reactive mercury in the manifold and systematic differences in the Tekran 2537/1130/1135 instruments) with this intercomparison experiment that still need to be resolved before the sampling protocols can be modified (Gustin et al., 2013). The issue of possible biases in the GOM measurements is currently under investigation (W. Luke, unpublished data). If this bias exists, it would affect the GOM measurements, but the GOM trend reported here likely remains valid. Because a consistent operation protocol has been followed for the operation of the Tekran systems since 2007, it is reasonable to assume that any biases in the GOM measurements would remain similar over this nine-year period as long as ozone and water vapor concentrations did not change significantly. This is the case as shown by the ozone and relative humidity data collected at the same site. The mean ozone concentration actually slightly increased at a rate of 0.2 ppbv $year^{-1}$ (not statistically significant though, p_value = 0.80), while the mean water mixing ratio remained essentially the same (Fig. S3). The slight ozone increase over 2007–2015 could have led to an increasing overestimation of GOM. Therefore the observed decrease in GOM would appear to be even more robust.

2.2.2. Ancillary measurements

Measurements of ancillary chemical species, including SO_2, O_3, CO, NO, and NO_y were made. Meteorological parameters such as temperature, relative humidity, precipitation, wind speed and direction, and solar radiation were also measured. Wet deposition of mercury was measured at the site according to the MDN protocols. Precipitation collectors gathered weekly samples for subsequent chemical analysis of total mercury, major ions, and trace metals. Weekly wet deposition was quantified by multiplying weekly precipitation totals by the total mercury concentrations measured in the weekly samples.

Table 1
Statistics of measured hourly concentrations of GEM, GOM, and PBM at the Beltsville site over 2007–2015. Minimum concentrations for GOM and PBM were zero (not shown).

Year	[GEM] (ng m^{-3})				[GOM] (pg m^{-3})			[PBM] (pg m^{-3})		
	Min	Max	Median	Mean ± std	Max	Median	Mean ± std	Max	Median	Mean ± std
2007	0.76	4.47	1.46	1.49 ± 0.29	254	3.1	8.0 ± 15.8	809	3.7	7.7 ± 24.6
2008	0.64	2.94	1.44	1.46 ± 0.24	430	1.9	7.2 ± 17.7	1009	5.7	7.8 ± 19.4
2009	0.47	18.1	1.32	1.33 ± 0.42	239	0.95	4.5 ± 10.7	438	3.7	6.7 ± 14.3
2010	0.88	21.1	1.41	1.45 ± 0.39	6848	1.3	5.3 ± 103	553	5.4	7.7 ± 17.1
2011	0.70	4.20	1.47	1.48 ± 0.21	140	1.0	3.0 ± 6.5	1677	4.7	7.1 ± 25.0
2012	0.49	3.94	1.43	1.43 ± 0.20	888	1.3	4.6 ± 18.0	7312	5.3	11.9 ± 136
2013	0.53	3.62	1.39	1.39 ± 0.22	250	0.65	2.9 ± 7.9	674	4.9	8.6 ± 22.8
2014	0.46	7.06	1.39	1.40 ± 0.29	390	1.5	4.8 ± 14.1	479	5.4	14.3 ± 27
2015	0.48	2.63	1.31	1.31 ± 0.19	235	1.26	3.8 ± 8.8	193	2.79	4.6 ± 7.5
All	**0.46**	**21.1**	**1.40**	**1.41 ± 0.23**	**6848**	**1.2**	**4.6 ± 33.7**	**7312**	**4.6**	**8.6 ± 56.8**

2.3. HYSPLIT back trajectory model

Five-day back trajectory simulations were conducted for hourly mercury measurements from 2007 to 2015 with the starting location initialized from the Beltsville site at the middle of the planetary boundary layer (PBL) with the starting time set to the midpoint of each sample hour. Back trajectories with high and low mercury concentrations observed at the site were compared to illustrate the transport history of the associated air masses and potential source-receptor relationships. The back trajectories were simulated using the NOAA's Hybrid Single-Particle Lagrangian Integrated Trajectory model (HYSPLIT) (Draxler and Rolph, 2015; Stein et al., 2015) and meteorological data from the North American Mesoscale (NAM) Forecast System model (Janjic et al., 2001; Janjic, 2003), with a horizontal resolution of 12 km, 26 vertical levels up to 20, 000 m (including 9 levels under 2000 m), and a time resolution of 3 h.

3. Results

3.1. Overall measurement statistics

A statistical summary of the mercury measurements at the Beltsville site from 2007 to 2015 is listed in Table 1. Mean concentrations and standard deviations of hourly measurements during this nine-year period were 1.41 ± 0.23 ng m^{-3} for GEM, 4.6 ± 33.7 pg m^{-3} for GOM, and 8.6 ± 56.8 pg m^{-3} for PBM. There were some variations in annual mean concentrations of GEM, GOM and PBM from year to year. Extreme GOM and PBM events were observed with the GOM concentration reaching 6.8 ng m^{-3} for 1 h in 2010 and the PBM concentration reaching 7.3 ng m^{-3} for 1 h in 2012.

Fig. 2 shows the frequency distributions of GEM, GOM, and PBM measurements at the Beltsville site from 2007 to 2015. The measurements of GEM show a nearly normal distribution while significant portions of GOM (38%) and PBM (7.6%) measurements are less than 0.5 pg m^{-3}.

3.2. Inter-annual variations

A decreasing inter-annual trend for GEM was observed at the Beltsville site from 2007 to 2015: 0.020 ± 0.007 ng m^{-3} yr^{-1} or 1.3 ± 0.5% yr^{-1} as shown in Fig. 3(a). This trend is statistically significant (p-value < 0.01) using a linear regression of simple t-test. A similar decreasing trend of GEM (i.e., 13% over the 2006–2014 period) was also observed at the Piney Reservoir air monitoring site in western Maryland located downwind of several large power plants in Ohio, Pennsylvania, and West Virginia (Castro and Sherwell, 2015). Quarterly mean concentrations of GEM measured at the Beltsville site typically ranged from 1.1 to 1.7 ng m^{-3}, mainly attributed to the seasonal variation as discussed in Section 3.3. The annual mean GEM concentrations ranged from 1.49 ng m^{-3} in 2007 to 1.31 ng m^{-3} in 2015 (Table 1). This variability may reflect an overall decreasing trend as well as potential meteorological and emission differences from year to year.

A statistically significant decreasing trend of 0.54 ± 0. 19 pg m^{-3} yr^{-1} or 7.3 ± 2.6% yr^{-1} for GOM (p-value < 0.01) was observed but there was no statistically significant trend for PBM even though there may be an apparent decrease (0.15 ± 0.35 pg m^{-3} yr^{-1} or 1.6 ± 3.8% yr^{-1}). Considerable variations are seen even for quarterly average values (Fig. 3(b) and (c)), with occasional episodes of high concentrations. The negative trend in

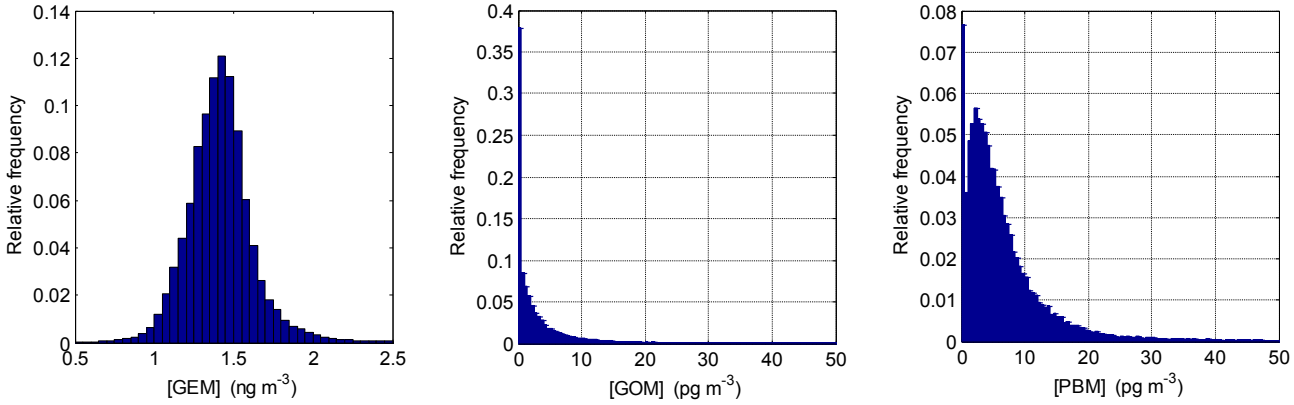

Fig. 2. Frequency distributions of hourly GEM (left), GOM (middle), and PBM (right) measurements at the Beltsville site from 2007 to 2015. All GEM, GOM, and PBM data, including zero values for GOM and PBM concentrations, are plotted. The sizes of the bins are 0.05 ng m^{-3} for GEM and 0.5 pg m^{-3} for GOM and PBM.

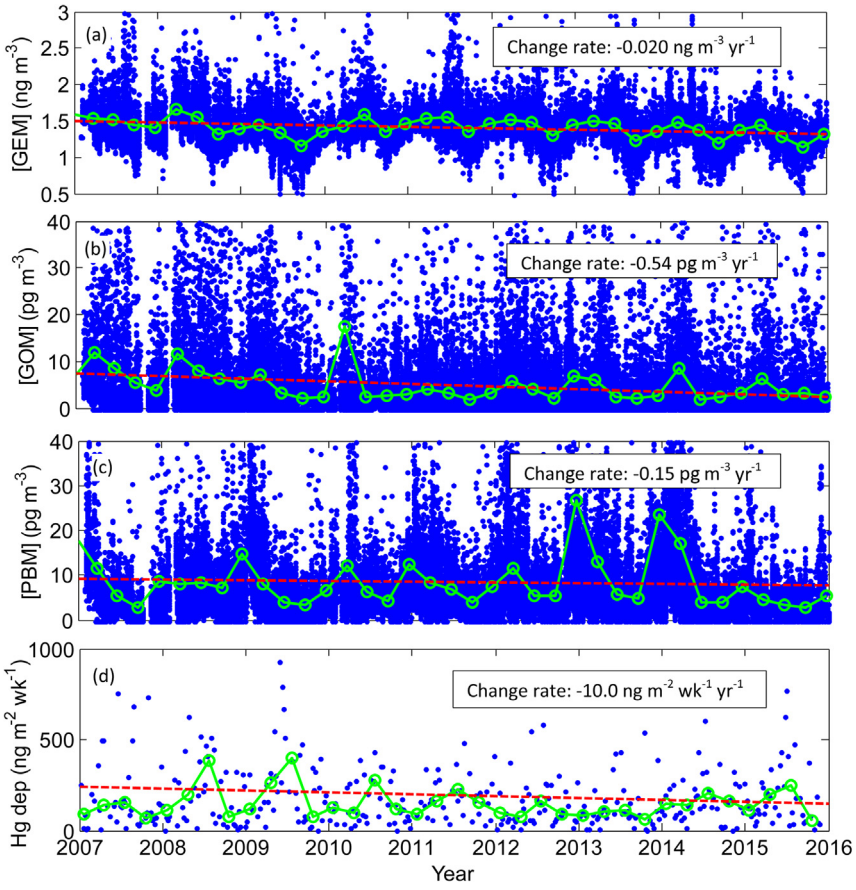

Fig. 3. Time series of GEM (a), GOM (b), PBM (c), and mercury wet deposition (d) measured at the Beltsville site in Maryland from 2007 to 2015. The individual points show hourly averaged atmospheric mercury concentrations in (a)–(c) and Hg wet deposition in weekly samples in (d). The linked green circles are quarterly mean mercury concentrations and Hg wet deposition. The red dashed lines represent linear regressions of the quarterly means over 2007–2015. (For interpretation of the references to colour in this figure legend, the reader is referred to the web version of this article.)

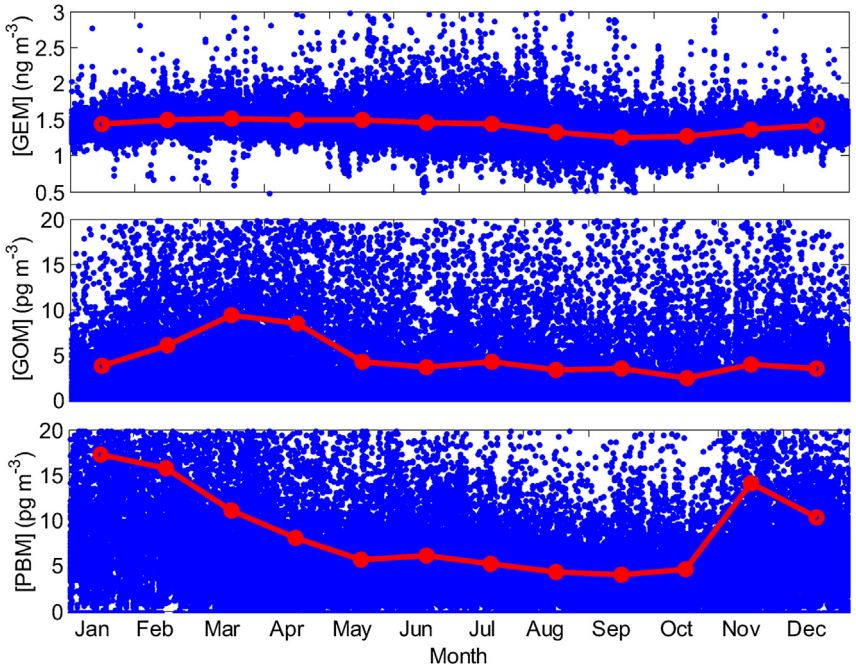

Fig. 4. Seasonal variations of GEM (top), GOM (middle), and PBM (bottom) measured at the Beltsville site in Maryland from 2007 to 2015. The individual points show 1-h data and the linked red circles are monthly mean values.

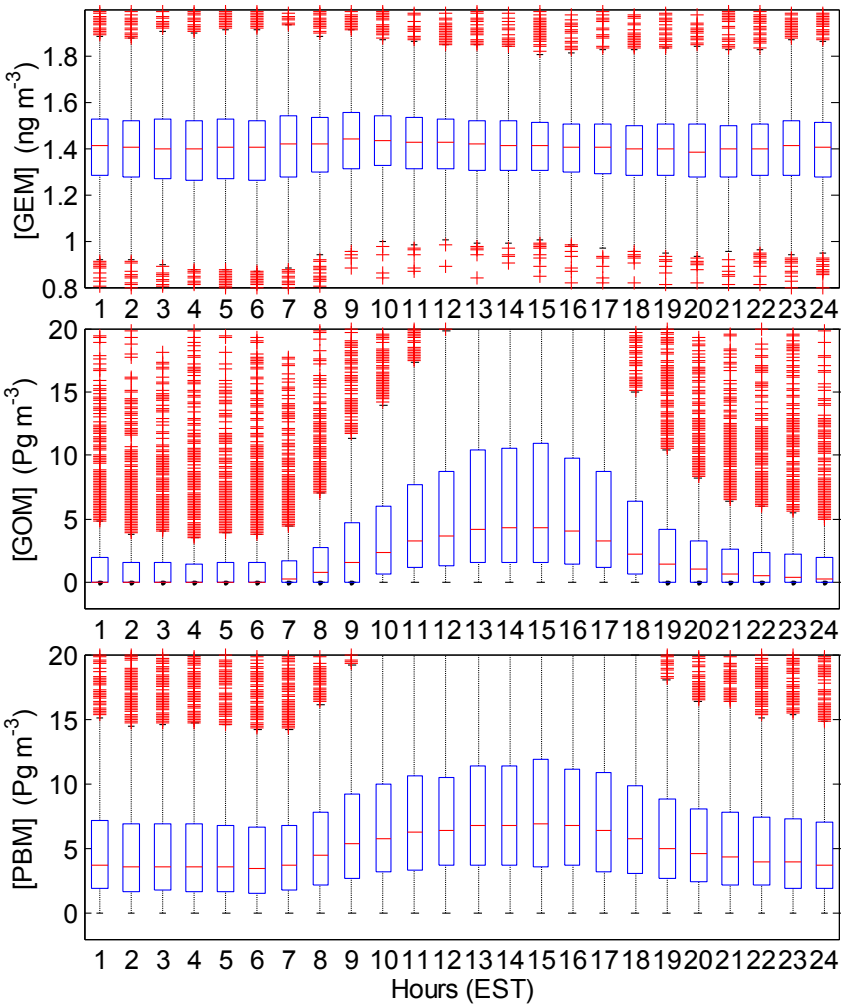

Fig. 5. Boxplots showing diurnal variations of GEM (top), GOM (middle), and PBM (bottom) measured at the Beltsville site in Maryland from 2007 to 2015. On each box, the central mark is the median, the edges of the box are the 25th and 75th percentiles, the whiskers extend to the most extreme data points not considered outliers, and outliers are plotted individually.

[GOM] could be partially due to fewer high GOM events in recent years.

The Hg wet deposition measured at the Beltsville site shows that there is also no statistically significant trend even though there is an apparent decrease of 10.0 ± 4.6 ng m^{-2} wk^{-1} yr^{-1} or 4.2 ± 1.9% yr^{-1} (p-value > 0.01). The rate of decrease in the Hg wet deposition is consistent with the decrease in GOM and PBM measured at the same site and the overall decrease in mercury

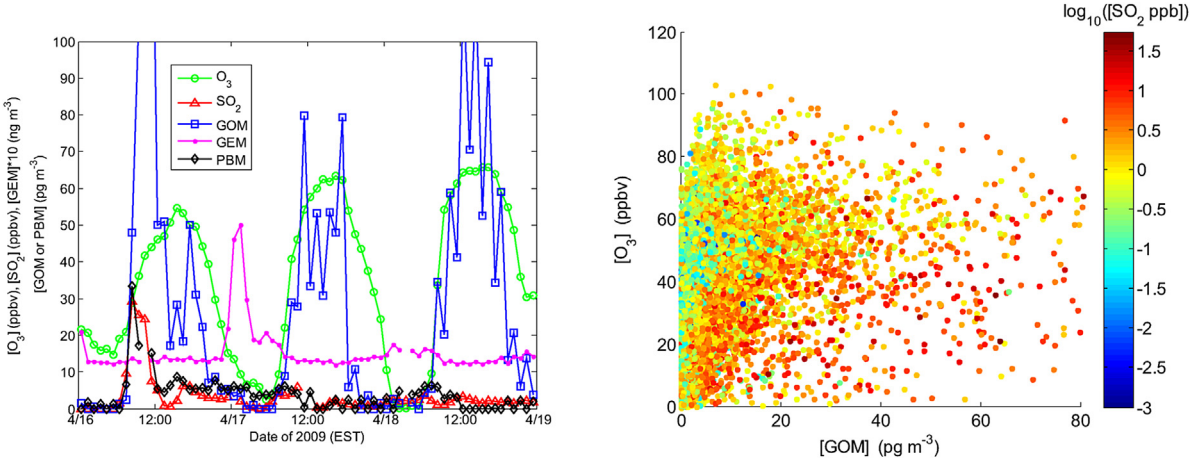

Fig. 6. Time series of ozone, SO_2, GEM, PBM, and GOM concentrations on three days in April 2009 (left) and ozone versus GOM colored with $\log_{10}$ ([SO_2 ppb]) (right) for the daytime data (with solar radiation greater than 10 W m^{-2}) collected from 2007 to 2015.

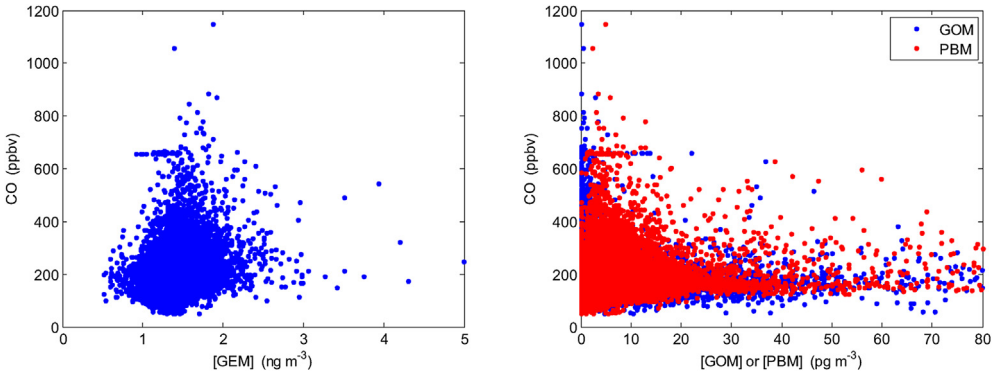

Fig. 7. Relationships between CO and GEM (left) and between CO and GOM/PBM (right) for the data collected at the Beltsville site from 2007 to 2015. Individual data points are hourly averaged measurements.

deposition at the MDN sites in Mid-Atlantic region (Weiss-Penzias et al., 2016).

3.3. Seasonal variations

Seasonal variations show that GEM concentrations were lowest in fall at the Beltsville site with the lowest monthly [GEM] of 1.24 ng m^{-3} observed in September, while GEM concentrations were generally constant in the other three seasons with a mean [GEM] of 1.45 ± 0.06 ng m^{-3} (Fig. 4). GOM concentrations were highest in spring with the highest monthly [GOM] of 9.3 pg m^{-3} was observed in March and generally constant in the other three seasons with a mean [GOM] of 3.8 ± 1.0 pg m^{-3}. The high [GOM] observed at the Beltsville site in spring may be associated to greater high pressure subsidence and a relatively long lifetime at the surface due to lower humidity in spring. This is consistent with the observations at several different sites in the southeastern United States (Nair et al., 2012; Gustin et al., 2012). PBM measurements exhibit higher levels from late fall to early spring with mean [PBM] of 12.7 ± 3.5 pg m^{-3} from November to April and lower levels from late spring to fall with a mean [PBM] of 4.9 ± 0.8 pg m^{-3} (Fig. 4). This season variation of PBM is consistent with some studies (e.g., Poissant et al., 2005; Nair et al., 2012; Xu et al., 2013; Schleicher et al., 2015) and may be in part due to increased gas to aerosol partitioning at lower temperatures and/or seasonal variations in emissions (e.g., due to varying fuel consumption patterns).

3.4. Diurnal variations

Diurnal variation of GEM concentrations at the Beltsville site is characterized by a slight peak in the morning with a median peak value of 1.43 ng m^{-3} at 9:00 Eastern Standard Time (EST) (Fig. 5). This is likely due to the confinement of emissions in the shallow boundary layer. Both GOM and PBM show strong diurnal variations with peaks in the afternoon, likely due to the production of reactive mercury from the photochemical oxidation of GEM. The maximum median hourly [GOM] of 4.4 pg m^{-3} and the maximum median hourly [PBM] of 6.7 pg m^{-3} appear both at 15:00 (EST). At night GOM concentrations were usually close to zero while PBM concentrations remained at a few pg m^{-3}. Similar diurnal variations of GEM, GOM, and PBM were observed at three types of sites (coastal suburban, urban and rural) in the southeast US (Nair et al., 2012; Gustin et al., 2012) as well as at a rural site in St. Anicet, Québec, Canada (Poissant et al., 2005). The diurnal variations of GEM, GOM, and PBM can also be influenced by the planetary boundary layer processes, e.g., mixing of GOM- and PBM-containing air down to the surface as the planetary boundary layer expands during midday (Gustin et al., 2012).

4. Discussion

4.1. Relationships between mercury and other chemical species

The relationships between GOM, ozone, and SO_2 can be used to differentiate GOM sources between direct emissions (with usually narrow plumes of SO_2 and GOM fumigating the site, leading to short-term spikes) and photochemical production (with longer term increases of GOM during midday) (Gustin et al., 2012; Ren et al., 2014). For example, on 16–18 April 2009, elevated GOM levels were observed (Fig. 6). In the morning of 16 April, simultaneous SO_2 and GOM spikes appeared with a peak [SO_2] of 30 ppbv and a peak [GOM] of 160 pg m^{-3}. After 11:30 EST on 16 April 2009,

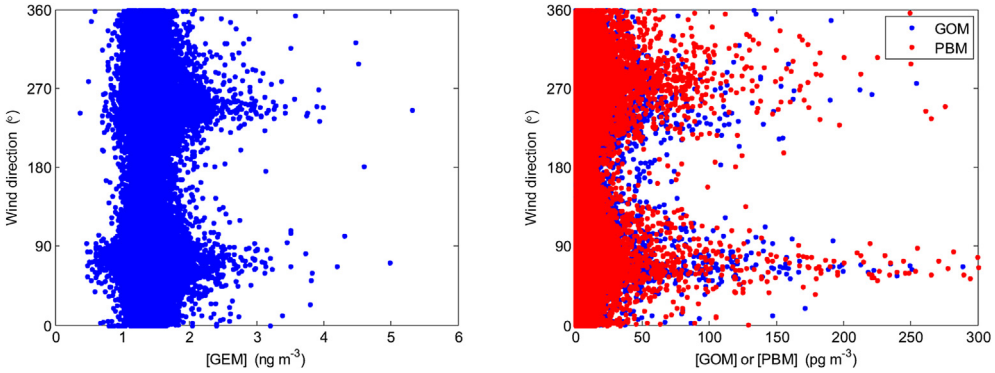

Fig. 8. Relationships between wind direction and GEM (left) and between wind direction and GOM or PBM (right). Individual data points are hourly averaged measurements.

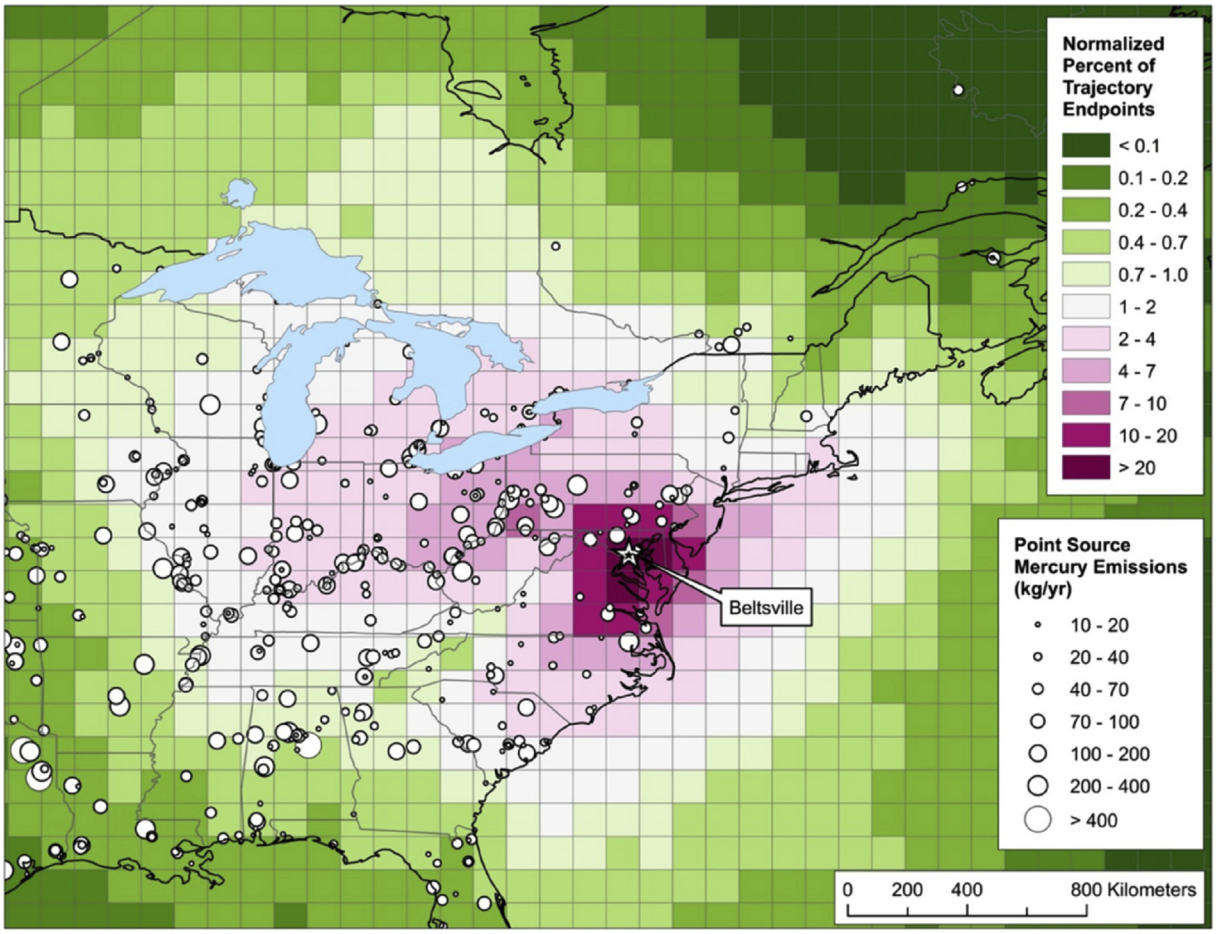

Fig. 9. Overall percent of endpoints passing through each 1°x1° grid square, normalized by the grid square with the maximum number of endpoints, for 120-h back-trajectories arriving at Beltsville, for the entire 2007–2015 period. Trajectory endpoints are only counted for a given grid point if the height of the endpoint is less than the HYSPLIT-estimated mixed-layer depth at that location and time. Year 2011 point-source total-mercury emissions data from the USEPA Toxic Release Inventory (TRI) and the Environment Canada National Pollutant Release Inventory (NPRI) are also shown. The color-blind-safe color ramp for this and subsequent maps was obtained from ColorBrewer.org (Brewer, 2016). (For interpretation of the references to colour in this figure legend, the reader is referred to the web version of this article.)

both SO_2 and GOM concentrations decreased sharply. On 17 and 18 April, SO_2 concentrations were generally low, about 1–2 ppbv, but a broad peak of GOM was observed on each day. This might suggest two different GOM production processes: direct emissions and photochemical production. The time series of GEM and PBM for the same time period also indicate these two distinct sources as a peak of PBM and a slight peak of GEM were observed in the morning of 16 April when the SO_2 peak appeared, while GEM and PBM remained relatively constant during the daytime of 17 and 18 April 2009. As shown by Poissant et al. (2005), increases in GOM by direct emissions were associated with increases in GEM and PBM, while photochemically produced GOM may not be associated with increases in GEM.

The relationship between ozone and GOM is simply a correlation and does not prove causation, i.e., these results do not prove that GEM is oxidized in sum or in part by ozone. There is substantial uncertainty regarding the overall relative importance of different potential GEM oxidizing agents (e.g., O_3, OH•, Br) and the spatio-temporal variability in relative importance (e.g., Ariya et al., 2015).

A scatter plot of ozone versus GOM colored by SO_2 concentrations may also suggest these two sources of GOM. High ozone and high GOM concentrations in general during the day (Fig. 6) might suggest photochemical production of GOM, while high GOM and SO_2 concentrations at low [O_3] might point to direct emissions of GOM. In addition, the diurnal change of the planetary boundary layer height might also possibly influence the diurnal variations of mercury species observed here.

High GEM and CO concentrations were both observed in general at the site even though the data points are scattered (Fig. 7). This is consistent with results from three sites in New Hampshire (Mao et al., 2012). Relationships between GOM and CO and between PBM and CO at Beltsville reveal that the highest GOM and PBM levels were observed in air masses with CO concentrations centered at ~200 ppbv (Fig. 7). This indicates that high GOM and PBM concentrations observed at this site likely existed in air masses that had continental origins, as opposed to marine-associated air masses, where CO concentrations are usually close to or below ~100 ppbv (Ou-Yang et al., 2014). It is also interesting to note that both GOM and PBM concentrations were not high (usually below ~20 pg m^{-3}) in the strongest CO plumes, typically encountered in the early morning or in the evening rush hour when photochemical processes were not active. This indicates different sources for CO and mercury with CO mainly coming from vehicular exhaust, but not much mercury coming from vehicular exhaust. The shallow boundary layer at night could also cause low concentrations of GOM due to its large deposition.

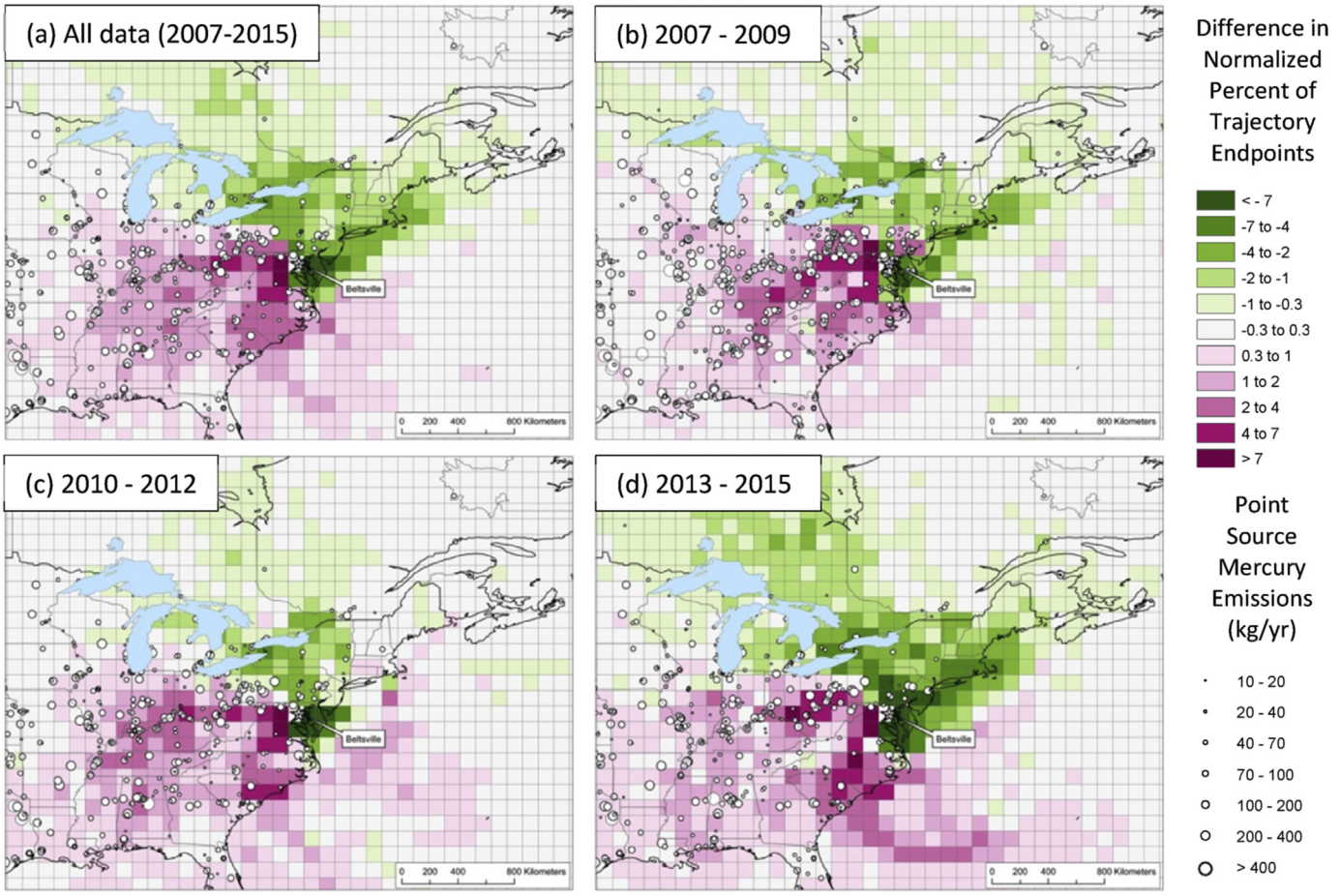

Fig. 10. Difference between the normalized percent of trajectory endpoints between the top 10% and bottom 10% of GEM concentrations, along with USEPA TRI and Environment Canada NPRI point-source total-mercury emissions data for (a) 2007–2015 (with 2011 emissions), (b) 2007–2009 (with 2008 emissions), (c) 2010–2012 (with 2011 emissions), and (d) 2013–2015 (with 2014 emissions). Positive numbers (purples) indicate that grid squares ($1^\circ \times 1^\circ$) were more likely to be encountered during high GEM concentration events. As with Fig. 9, trajectory endpoints are only counted for a given grid point if the height of the endpoint is less than the HYSPLIT-estimated mixed-layer depth at that location and time. (For interpretation of the references to colour in this figure legend, the reader is referred to the web version of this article.)

4.2. Correlation with meteorological parameters

Wind direction played an important role in enhanced GEM, GOM, and PBM concentrations observed at the Beltsville site. As shown in Fig. 8, the highest concentrations of GEM, GOM, and PBM were mainly observed in air masses from two wind sectors: westerly (from southwesterly to northwesterly) and easterly/northeasterly. This is expected as major coal-fired power plants, which have significant mercury emissions, are mainly found in these two wind sectors from the site. Several large power plants are located to the west of the site in the Ohio River Valley area in Ohio, Pennsylvania, and West Virginia (Fig. 1). The Brandon Shores Power Plant in Maryland lies approximately 30 km to the northeast of the site and could significantly affect measured mercury concentrations in northeasterly flow. Since the wind direction at the site will not necessarily reflect the transport over the entire pathway from any given source to the site, a back-trajectory analysis (described in Section 4.3) was performed to address this issue.

4.3. Back trajectory frequency analysis

The overall, gridded trajectory frequencies over 2007–2015 (Fig. 9) show the general, regional pattern of air mass pathways that could influence the mercury measurements at the site. This figure shows the percent of 10-min endpoints passing through each 1^ox1^o grid square. To identify potential source regions impacting the site, two groups of back trajectories for the highest and lowest concentrations of each form of mercury (Fig. 2) were selected. The spatial distribution of cell-by-cell frequency difference between the high-concentration group and the low-concentration group of trajectories for each form of mercury can then be used to assess any differences in the pathways of air masses associated with high and low mercury concentrations at the site. Similar approaches have been used in other studies to examine potential source-receptor relationships (e.g., Rolison et al., 2013; Ren et al., 2014; Venter et al., 2015). In the overall trajectory frequency results shown in Fig. 9 and in the subsequent frequency difference results discussed below, an endpoint was attributed to a given cell only if its height was within the model-estimated PBL at that time.

4.3.1. GEM

The differences of trajectory frequencies for the top 10% of [GEM] and the bottom 10% of [GEM] are shown in Fig. 10. The GEM data for the entire nine-year period were used, as well as for each three-year period (2007–2009, 2010–2012, and 2013–2015) to see the co-benefits of the emission controls implemented since around 2009 for power plants in the region to meet the US EPA's Clean Air Interstate Rule, a cap and trade program designed to reduce SO_2 and nitrogen oxides (NO_x) emissions from power plants in the eastern United States (US EPA, 2015). In Fig. 10, the areas with

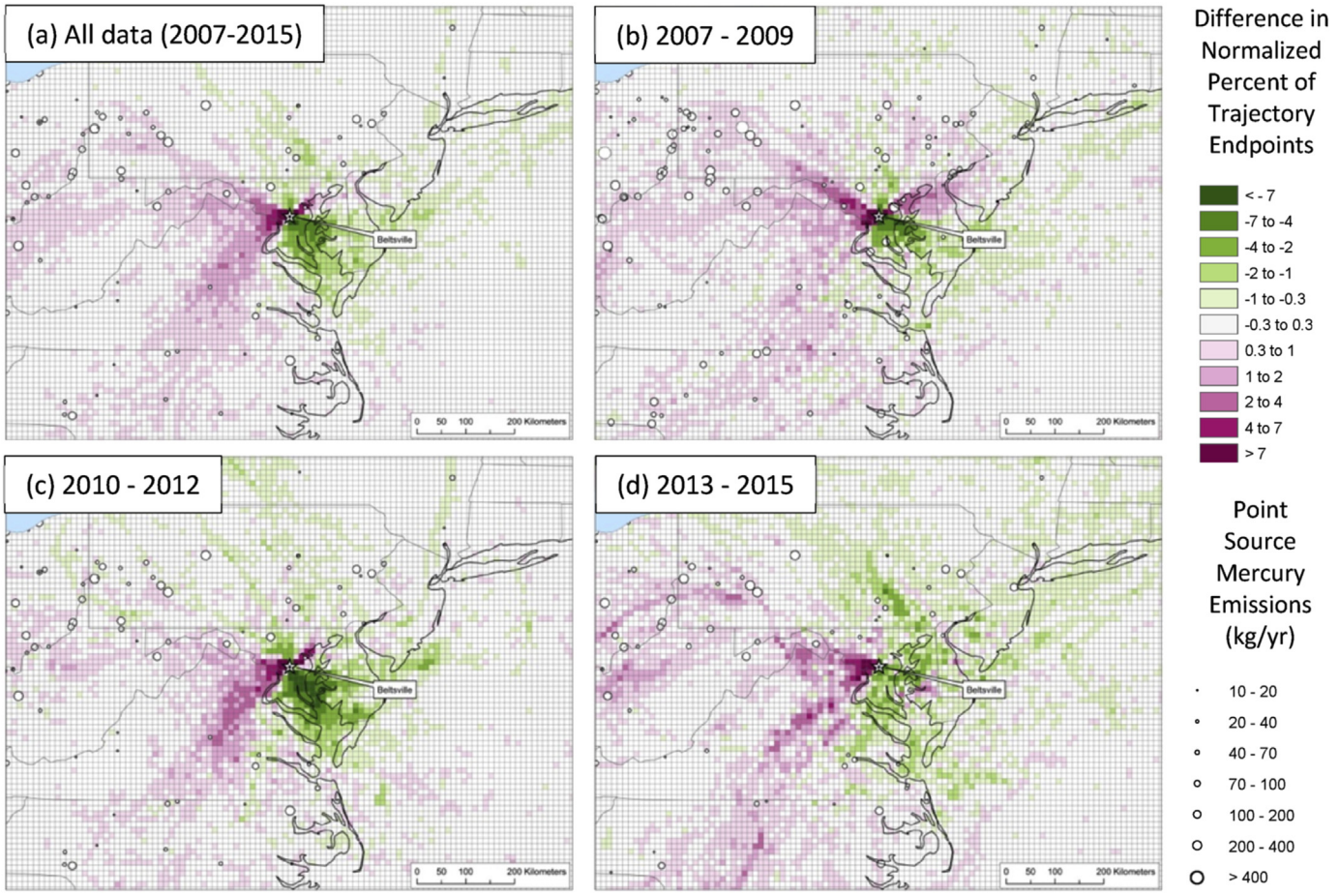

Fig. 11. Same as Fig. 10 but with a finer spatial scale and 0.1° × 0.1° grid cells. (For interpretation of the references to colour in this figure legend, the reader is referred to the web version of this article.)

positive frequency differences (purple) mean that back-trajectories for high [GEM] have a greater chance passing through these areas than back-trajectories for low [GEM], while the areas with negative frequency differences (green) mean that back-trajectories for low [GEM] have a greater chance passing through these areas than back-trajectories for high [GEM].

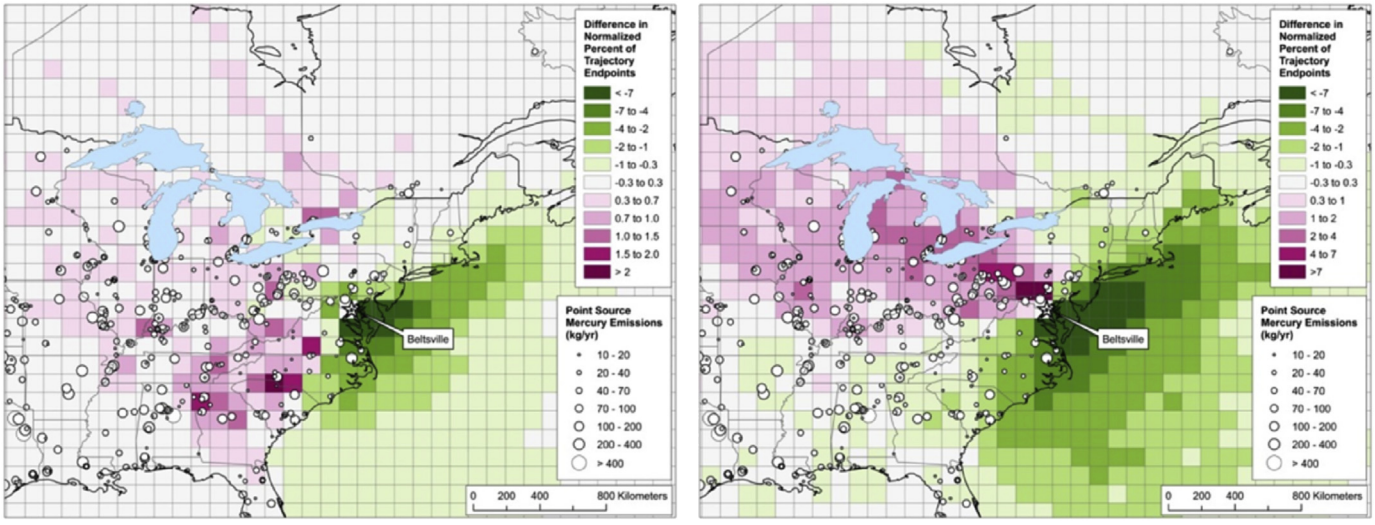

Fig. 12. Difference between the normalized percent of trajectory endpoints between the top 10% and bottom 38% of GOM concentrations (left) and between the top 10% and bottom 10% of PBM concentrations (right) over 2007–2015. Positive numbers (purples) indicate that grid squares were more likely to be encountered during high concentration events. USEPA TRI and Environment Canada NPRI point-source total-mercury emissions for 2011 are also shown. As with Figs. 9–11, trajectory endpoints are only counted for a given grid point if the height of the endpoint is less than the HYSPLIT-estimated mixed-layer depth at that location and time. (For interpretation of the references to colour in this figure legend, the reader is referred to the web version of this article.)

Fig. 10 shows that regions to the west and southwest of the site, where most major power plants are located, correspond with trajectories of air masses that reached the site with higher GEM concentrations. The decline in [GEM] observed at the Beltsville site may be due to mercury emissions reductions from sources in these regions. Mercury emissions from coal-fired power plants throughout the region have decreased due to a combination of pollution control additions, fuel changes from coal to natural gas, and plant shutdowns (Figs. S4 and S5). For example, according to the Air Markets Program Data of US EPA (http://www.ampd.epa.gov/ampd/), SO_2 emissions from power plants in Maryland, Delaware, Virginia, West Virginia, Pennsylvania, and Ohio have been reduced by ~12% yr^{-1} from 2007 to 2015. While the emissions have declined and lower mercury concentrations have been observed, the mercury concentrations were still relatively high in the air coming from large source regions.

There may also be some evidence of the importance of marine GEM emissions, especially during 2013–2015 (Fig. 10(d)). Given that global net oceanic emissions of GEM are comparable to global anthropogenic emissions (e.g., Pirrone et al., 2010), this is not necessarily unexpected. Air masses advected from the north and northeast were generally associated with lower GEM concentrations, except as noted immediately below. Northerly air masses reaching the site with low GEM levels are likely associated with clean air coming from Canada, especially after the passage of cold fronts.

During 2007–2009, a portion of high GEM events were associated with high frequencies of the trajectories passing through areas to the northeast of the site (Fig. 11(b)), while the area associated with this portion of high trajectory frequencies was reduced in 2010–2012 (Fig. 11(c)) and completely disappeared in 2013–2015 (Fig. 11(d)). This change may be due to recent emission reductions in the region northeast of the site. Mercury emissions from the Brandon Shores/Wagner power plant (30 km northeast of the site) and the C.P. Crane power plant (51 km northeast of the site) decreased from a total of ~300 kg yr^{-1} in 2008 to 130 kg yr^{-1} in 2009 to less than 50 kg yr^{-1} in 2010 and subsequent years (Fig. S5).

4.3.2. GOM and PBM

We first note that the use of back-trajectories to interpret GOM or PBM represents a significant oversimplification due to the relatively short atmospheric lifetimes of these mercury forms in the atmosphere. Trajectories do not account for deposition processes that occur along the air parcel pathway. For GEM, with an atmospheric lifetime of ~6–12 months, these processes are less important than for GOM and PBM, with lifetimes on the order of days (GOM) to 1–2 weeks (PBM) in the boundary layer. Nevertheless, trajectory analysis may provide some aid to interpreting observations at the site. Accordingly, a trajectory frequency analysis comparable to that carried out for GEM was performed for GOM and PBM (Fig. 12). As in the above figures, positive frequency differences (purple) represent areas where back-trajectories associated with high [GOM] (or [PBM]) have a greater chance of passing through than those areas associated with low [GOM] (or [PBM]) (and vice versa for the green-shaded grid squares representing negative frequency differences). Frequency differences for PBM show a more pronounced pattern of arrival from areas to the north and west of the site. For GOM, the pattern is more diffuse, and the positive frequency differences are generally smaller. The differences between the apparent footprints of high [GOM], [PBM], and [GEM] back trajectory frequencies impacting the site demonstrate the complex – and as yet incompletely understood – interplay between emissions and atmospheric fate and transport affecting ambient mercury concentrations at the Beltsville site.

5. Conclusions

Nine years of continuous measurements of operationally defined mercury forms have been made at the Beltsville site in Maryland from 2007 to 2015. This suburban site was affected by regional emission sources of mercury and other primary trace species with occasional transport-related episodes of higher concentrations.

GEM concentration at the Beltsville site has been decreasing during this nine-year period with a decrease rate of 0.020 ± 0.007 ng m^{-3} yr^{-1} (or 1.3 ± 0.5% yr^{-1}, statistically significant, p-value < 0.01). Diurnal variation of GEM concentration shows a slight peak in the morning. Seasonal variation of GEM shows lower levels in fall. GOM concentration has also been decreasing with a decrease rate of 0.54 ± 0.19 pg m^{-3} yr^{-1} (or 7.3 ± 2.6% yr^{-1}, statistically significant, p-value < 0.01) during this nine-year period, while the decrease rate for PBM concentration (0.15 ± 0.35 pg m^{-3} yr^{-1} or 1.6 ± 3.8% yr^{-1}) was not statistically significant (p-value > 0.01). Coincident with the decreases in the atmospheric mercury concentrations, the Hg wet deposition has been decreasing at a rate of 10.0 ± 4.6 ng m^{-2} wk^{-1} yr^{-1} (or 4.2 ± 1.9% yr^{-1}), although it is not statistically significant with a p-value > 0.01. Seasonally, GOM measurements show high levels in spring and consistently low levels in the other three seasons, while PBM measurements exhibit higher levels from late fall to early spring and lower levels from late spring to fall. Both diurnal variations of GOM and PBM show peaks in the afternoon likely due to the production of reactive mercury from the photochemical oxidation of GEM but possibly also due to the change of the planetary boundary layer height.

This study indicates that the receptor site experienced impacts from mercury sources that are both local and regional in nature. Relationships between elevated GEM/GOM/PBM and wind direction indicate mercury measurements at this site may be influenced by nearby mercury sources. Back trajectory frequency analyses suggest potential relationships between mercury emissions and observed high concentrations of GEM, GOM, and PBM at this site, but the source-receptor relationships are varied and complex. Relationships among GOM, ozone and SO_2 might suggest two sources of GOM: direct emissions from mercury sources and in situ photochemical production.

Acknowledgments

We are grateful to Daniel Tong, Glenn Rolph, Barbara Stunder, Fantine Ngan, and Tianfeng Chai at NOAA Air Resources Laboratory for helpful discussions. This work was supported by NOAA, US Environmental Protection Agency, and Maryland Department of Natural Resources. In addition, the authors would like to express their appreciation to three anonymous reviewers who provided insightful comments and helpful suggestions which have improved this paper.

Appendix A. Supplementary data

Supplementary data related to this article can be found at http://dx.doi.org/10.1016/j.atmosenv.2016.08.028.

References

Ambrose, J.L., Lyman, S.N., Huang, J., Gustin, M.S., Jaffe, D.A., 2013. Fast time resolution oxidized mercury measurements during the Reno atmospheric mercury intercomparison experiment (RAMIX). Environ. Sci. Technol. 47, 7285–7294.

Ariya, P.A., Amyot, M., Dastoor, A., Deeds, D., Feinberg, A., Kos, G., Poulain, A., Ryjkov, A., Semeniuk, K., Subir, M., Toyota, K., 2015. Mercury physicochemical and biogeochemical transformation in the atmosphere and at atmospheric

interfaces: a review and future directions. Chem. Rev. 115, 3760–3802.
Aspmo, K., Gauchard, P.-A., Steffen, A., Temme, C., Berg, T., Bahlmann, E., Banic, C., Dommergue, A., Ebinghaus, R., Ferrari, C., Pirrone, N., Sprovieri, F., Wibetoe, G., 2005. Measurements of atmospheric mercury species during an international study of mercury depletion events at Ny-Ålesund, Svalbard, spring 2003. How reproducible are our present methods? Atmos. Environ. 39, 7607–7619.
Brewer, C., 2016. ColorBrewer.org Website. http://colorbrewer2.org (accessed 26 06 2016).
Castro, M.S., Sherwell, J., 2015. Effectiveness of emission controls to reduce the atmospheric concentrations of mercury. Environ. Sci. Technol. 49, 14000–14007.
Choi, A.L., Grandjean, P., 2008. Methylmercury exposure and health effects in humans. Environ. Chem. 5, 112–120.
Draxler, R.R., Rolph, G.D., 2015. HYSPLIT (HYbrid Single-particle Lagrangian Integrated Trajectory) Model. NOAA Air Resources Laboratory, Maryland, MD, USA. Available online: http://ready.arl.noaa.gov/HYSPLIT.php (accessed 25 11 2015).
Fitzgerald, W.F., Engstrom, D.R., Mason, R.P., Nater, E.A., 1998. The case for atmospheric mercury contamination in remote areas. Environ. Sci. Technol. 3, 1–7.
Fu, X.W., Zhang, H., Yu, B., Wang, X., Lin, C.J., Feng, X.B., 2015. Observations of atmospheric mercury in China: a critical review. Atmos. Chem. Phys. 15, 9455–9476.
Gay, D.A., Schmeltz, D., Prestbo, E., Olson, M., Sharac, T., Tordon, R., 2013. The Atmospheric Mercury Network: measurement and initial examination of an ongoing atmospheric mercury record across North America. Atmos. Chem. Phys. 13, 11,339–11,349.
Gustin, M.S., Weiss-Penzias, P.S., Peterson, C., 2012. Investigating sources of gaseous oxidized mercury in dry deposition at three sites across Florida, USA. Atmos. Chem. Phys. 12, 9201–9219.
Gustin, M.S., Huang, J., Miller, M.B., Peterson, C., Jaffe, D.A., Ambrose, J., Finley, B.D., Lyman, S.N., Call, K., Talbot, R., Feddersen, D., Mao, H., Lindberg, S.E., 2013. Do we understand what the mercury speciation instruments are actually measuring? Results of RAMIX. Environ. Sci. Technol. 47, 7295–7306.
Janjic, Z.I., Gerrity Jr., J.P., Nickovic, S., 2001. An alternative approach to nonhydrostatic modeling. Mon. Weather Rev. 129, 1164–1178.
Janjic, Z.I., 2003. A nonhydrostatic model based on a new approach. Meteorol. Atmos. Phys. 82, 271–285.
Landis, M.S., Stevens, R.K., Schaedlich, F., Prestbo, E.M., 2002. Development and characterization of an annular denuder methodology for the measurement of divalent inorganic reactive gaseous mercury in ambient air. Environ. Sci. Technol. 36, 3000–3009.
Lindberg, S., Brooks, S., Lin, C.-J., Scott, K., Landis, M., Stevens, R., Goodsite, M., Richter, A., 2002. Dynamic oxidation of gaseous mercury in the Arctic troposphere at polar sunrise. Environ. Sci. Technol. 36, 1245–1256.
Lyman, S.N., Jaffe, D.A., Gustin, M.S., 2010. Release of mercury halides from KCl denuders in the presence of ozone. Atmos. Chem. Phys. 10, 8197–8204.
Mao, H., Talbot, R., Hegarty, J., Koermer, J., 2012. Speciated mercury at marine, coastal, and inland sites in New England - Part 2: relationships with atmospheric physical parameters. Atmos. Chem. Phys. 12, 4181–4206.
McClure, C.D., Jaffe, D.A., Edgerton, E.S., 2014. Evaluation of the KCl denuder method for gaseous oxidized mercury using $HgBr_2$ at an in-service AMNet site. Environ. Sci. Technol. 48, 11,437–11,444.
Morel, F.M.M., Kraepiel, A.M.L., Amyot, M., 1998. The chemical cycle and bioaccumulation of mercury. Annu. Rev. Ecol. Syst. 29, 543–566.
National Atmospheric Deposition Program (NADP)'s Mercury Deposition Network (MDN), Monitoring mercury deposition: A key tool to understanding the link between emissions and effects. Available online: http://nadp.sws.uiuc.edu/lib/brochures/mdn.pdf (accessed 15 12 2015).
Nair, U.S., Wu, Y., Walters, J., Jansen, J., Edgerton, E.S., 2012. Diurnal and seasonal variation of mercury species at coastal-suburban, urban, and rural sites in the southeastern United States. Atmos. Environ. 47, 499–508.
Ou-Yang, C.F., Lin, N.H., Lin, C.C., Wang, S.H., Sheu, G.R., Lee, C.T., Schnell, R.C., Lang, P.M., Kawasato, T., Wang, J.L., 2014. Characteristics of atmospheric carbon monoxide at a high-mountain background station in East Asia. Atmos. Environ. 89, 613–622.
Pirrone, N., Cinnirella, S., Feng, X., Finkelman, R.B., Friedli, H.R., Leaner, J., Mason, R., Mukherjee, A.B., Stracher, G.B., Streets, D.G., Telmer, K., 2010. Global mercury emissions to the atmosphere from anthropogenic and natural sources. Atmos. Chem. Phys. 10, 5951–5964.
Poissant, L., Pilote, M., Beauvais, C., Constant, P., Zhang, H.H., 2005. A year of continuous measurements of three atmospheric mercury species (GEM, RGM and Hg p) in southern Quebec, Canada. Atmos. Environ. 39, 1275–1287.
Ren, X., Luke, W.T., Kelley, P., Cohen, M., Ngan, F., Artz, R., Walker, J., Brooks, S., Moore, C., Swartzendruber, P., Bauer, D., Remeika, J.A., Hynes, J., Dibb, J., Rolison, J., Krishnamurthy, N., Landing, W.M., Hecobian, A., Shook, J., Huey, L.G., 2014. Mercury speciation at a coastal site in the northern Gulf of Mexico: results from the Grand Bay intensive studies in summer 2010 and spring 2011. Atmosphere 5, 230–251.
Rolison, J.M., Landing, W.M., Luke, W., Cohen, M., Salters, V.J.M., 2013. Isotopic composition of species-specific atmospheric Hg in a coastal environment. Chem. Geol. 336, 37–49.
Schleicher, N.J., Schafer, J., Blanc, G., Chen, Y., Chai, F., Cen, K., Norra, S., 2015. Atmospheric particulate mercury in the megacity Beijing: Spatiotemporal variations and source apportionment. Atmos. Environ. 109, 251–261.
Schroeder, W.H., Munthe, J., 1998. Atmospheric mercury-an overview. Atmos. Environ. 32, 809–822.
Selin, N.E., 2009. Global biogeochemical cycling of mercury: a review. Ann. Rev. Environ. Res. 34, 43–63.
Sprovieri, F., Pirrone, N., Ebinghaus, R., Kock, H., Dommergue, A., 2010. A review of worldwide atmospheric mercury measurements. Atmos. Chem. Phys. 10, 8245–8265.
Stein, A.F., Draxler, R.R., Rolph, G.D., Stunder, B.J.B., Cohen, M.D., Ngan, F., 2015. NOAA's HYSPLIT atmospheric transport and dispersion modeling system. Bull. Amer. Meteor. Soc. 96, 2059–2077.
Sunderland, E., 2007. Mercury exposure from domestic and imported estuarine and marine fish in the U.S. Seafood Market. Environ. Health Perspect. 115, 235–242.
Temme, C., Blanchard, P., Steffen, A., Banic, C., Beauchamp, S., Poissant, L., Tordon, R., Wiens, B., 2007. Trend, seasonal and multivariate analysis study of total gaseous mercury data from the Canadian atmospheric mercury measurement network (CAMNet). Atmos. Environ. 41, 5423–5441.
UNEP. Global Mercury Assessment, 2013. Sources, Emissions, Releases and Environmental Transport. UNEP Chemicals Branch, Geneva, Switzerland. Available online: http://www.unep.org/PDF/PressReleases/GlobalMercuryAssessment2013.pdf.
U.S. Environmental Protection Agency (US EPA), 2016. Clean Air Status and Trends Network (CASTNET), hourly ozone, SO2, CO, and meteorological data. Available at: http://www.epa.gov/castnet (accessed 15 January, 2016).
United States Environmental Protection Agency (US EPA) Website: http://archive.epa.gov/airmarkets/programs/cair/web/html/index.html (accessed 15 12 2015).
Venter, A.D., Beukes, J.P., van Zyl, P.G., Brunke, E.G., Labuschagne, C., Slemr, F., Ebinghaus, R., Kock, H., 2015. Statistical exploration of gaseous elemental mercury (GEM) measured at Cape Point from 2007 to 2011. Atmos. Chem. Phys. 15, 10271–10280.
Weiss-Penzias, P.S., Gay, D.A., Brigham, M.E., Parsons, M.T., Gustin, M.S., Schure, A.T., 2016. Trends in mercury wet deposition and mercury air concentrations across the U.S. and Canada. Sci. Total Environ. http://dx.doi.org/10.1016/j.scitotenv.2016.01.061.
Xu, L.L., Chen, J.S., Niu, Z.C., Yin, L.Q., Chen, Y.T., 2013. Characterization of mercury in atmospheric particulate matter in the southeast coastal cities of China. Atmos. Pollut. Res. 4, 454–461.
Zhang, Y., Jacob, D.J., Horowitz, H.M., Chen, L., Amos, H.M., Krabbenhoft, D.P., Slemr, F., St Louis, V.L., Sunderland, E.M., 2016. Observed decrease in atmospheric mercury explained by global decline in anthropogenic emissions. Proc. Natl. Acad. Sci. 113, 526–531.